

# Macroscopic production of highly nuclear-spin-polarized molecules from IR-excitation and photodissociation of molecular beams

C. S. Kannis<sup>a,b</sup>, T. P. Rakitzis<sup>b,c,\*</sup>

<sup>a</sup>*Institute for Nuclear Physics, Forschungszentrum Jülich, 52425 Jülich, Germany*

<sup>b</sup>*University of Crete, Department of Physics, Herakleio, Greece*

<sup>c</sup>*Foundation for Research and Technology Hellas, Institute of Electronic Structure and Laser, N. Plastira 100, Heraklion, Crete, Greece, GR-71110*

---

## Abstract

Pure, highly nuclear-spin-polarized molecules have only been produced with molecular beam-separation methods, with production rates up to  $\sim 3 \times 10^{12} \text{ s}^{-1}$ . Here, we propose the production of spin-polarized molecular photofragments from the IR-excitation and photodissociation of molecular beams, with production rates approaching the tabletop-IR-laser photon fluxes of  $10^{21} \text{ s}^{-1}$ . We give details on the production of spin-polarized molecular hydrogen and water isotopes, from formaldehyde and formic acid beams, respectively. Macroscopic quantities of these molecules are important for NMR signal enhancement, and for the needs of a nuclear fusion reactor, to increase the D-T or D- $^3\text{He}$  unpolarized nuclear fusion cross section by  $\sim 50\%$ .

*Keywords:* nuclear-spin-polarized molecules, molecular beams, IR excitation, photodissociation, molecular hyperpolarization

*2010 MSC:* 00-01, 99-00

---

## <sup>1</sup> 1. Introduction

<sup>2</sup> The production of nuclear spin polarization is important in several  
<sup>3</sup> fields, including the study of spin-dependent effects in particle and nuclear

---

\*Corresponding author

URL: [ptr@iesl.forth.gr](mailto:ptr@iesl.forth.gr) (T. P. Rakitzis)

4 physics [1], and in applications of nuclear magnetic resonance (NMR)  
5 [2, 3, 4]. However, current methods for producing highly spin-polarized  
6 molecules, such as molecular-beam separation techniques, polarization  
7 through “brute force” cryogenic cooling, dynamic nuclear polarization  
8 (DNP), and pulsed-laser excitation of molecular beams, have significant  
9 production and polarization limitations for many applications.

10 “Brute force” cryogenic cooling of solid D<sub>2</sub> to 35 mK in a 14.5 T field,  
11 produces a polarization of only about 13% [5]. For 100% polarized nuclei,  
12 The D-T and D-<sup>3</sup>He nuclear-fusion reaction cross sections are enhanced by  
13 50% [6], and may increase the reactor efficiency by ~75% [7]. A GW nuclear  
14 fusion reactor will need ~10<sup>21</sup> s<sup>-1</sup> of 100% polarized D to benefit fully from  
15 this effect [8, 9, 10]. Therefore, the “brute force” method cannot produce  
16 sufficiently polarized D for this application.

17 In DNP, the unpaired electrons in free radicals are highly polarized at  
18 low temperature in a magnetic field, and this polarization is transferred to  
19 the nuclei of the target sample [11]. This works successfully for a wide  
20 range of molecules, however the removal of the radicals, necessary for *in*  
21 *vivo* NMR applications, is difficult and can significantly lower the sample  
22 polarization [12].

23 Molecular-beam separation techniques, using electric or magnetic  
24 field gradients, is the only method that can produce pure, ~100%  
25 nuclear-spin-polarized molecules, however only microscopic production rates  
26 have been demonstrated of ~3×10<sup>12</sup> for ortho-H<sub>2</sub> and ~5×10<sup>11</sup> s<sup>-1</sup> for  
27 ortho-D<sub>2</sub> [13], and below ~10<sup>9</sup> for ortho-H<sub>2</sub>O [14, 15], many orders of  
28 magnitude lower than required for many applications; for example, NMR  
29 applications and tests of polarized fusion require production rates of at least  
30 10<sup>17</sup> s<sup>-1</sup>.

31 The single-photon rovibrational excitation of molecular beams with an IR  
32 laser pulse [16, 17], followed by transfer of the rotational polarization to the  
33 nuclear spin via the hyperfine interaction, has been shown to polarize highly  
34 the nuclear spins of isolated molecules. This method of hyperpolarization  
35 has been demonstrated for Cl nuclei in HCl molecules [18, 19]. However,  
36 a path for high production rates for important nuclei, such as H/D/T, was  
37 not shown; also, high polarization was not demonstrated for H isotopes via  
38 IR excitation, as the rotational polarization preferentially polarizes the more  
39 strongly coupled Cl nucleus first. The biggest problem is that only isolated  
40 spin-polarized atoms have been produced with this method, and that the  
41 production of spin-polarized molecules (such as H<sub>2</sub> isotopes) have only been

42 performed by recombining the polarized atoms at a surface [20]; this is a very  
43 complicated extra step, which has not been demonstrated at high production  
44 rates.

45 Here, we propose improvements to the rovibrational excitation method  
46 that will allow macroscopic production rates of pure, highly-polarized  
47 molecules ( $\sim 100\%$ ), at rates that can approach the photon fluxes of the IR  
48 excitation step. The improvements are motivated by the recent availability  
49 of tabletop tunable, narrow-bandwidth, high-power IR lasers, producing  
50  $\sim 10^{21}$  photons  $s^{-1}$  [21], and are: (i) optical excitation steps that allow *only*  
51 molecules with 100% nuclear polarization to be photodissociated, providing  
52 a pure polarization spin filter, and (ii) excitation and polarization of larger  
53 molecules which can be photodissociated to yield exclusively polarized  
54 molecular photofragments, without needing to recombine polarized atoms;  
55 this is particularly important for molecules that are not IR active (such  
56 as  $H_2$  isotopes), and cannot be excited directly. Specifically, we propose  
57 the IR-excitation of the special cases of formaldehyde ( $CH_2O$ ) or formic  
58 acid ( $CH_2O_2$ ), which can be photodissociated to yield exclusively the  $H_2$   
59 + CO [22] or  $H_2O$  + CO [23] channels, respectively. The target molecules  
60 (here  $H_2$  or  $H_2O$  isotopes) can then be selectively trapped at a surface.  
61 Thus, we propose the production of macroscopic quantities of  $\sim 100\%$   
62 nuclear-spin-polarized isotopes of hydrogen molecules ( $H_2$ , HD, DT) and  
63 water molecules ( $H_2O$ ,  $D_2O$ ), which are important for the applications of  
64 polarized nuclear fusion and NMR signal enhancement. This production  
65 method will surpass conventional beam separation methods by several orders  
66 of magnitude, and may approach the photon flux of the IR excitation lasers  
67 (details given below).

68 Below, and in Figs. 1 and 2, we give details on the production of  $\sim 100\%$   
69 nuclear-spin-polarized molecules from IR-excitation and photodissociation of  
70  $CH_2O$  and  $CH_2O_2$ . The steps are described generally, but specific numbers  
71 are given for the case of  $CH_2O$  (for production rates of up to  $10^{20}$   $s^{-1}$   
72 spin-polarized  $H_2$ ):

73 1. *Slit nozzle supersonic expansion.* Produces a  $10\text{ cm} \times 1\text{ cm}$  jet at the  
74 laser interaction region (Fig. 1 and [24]), with  $CH_2O$  density of  $\sim 2 \times 10^{15}$   
75  $\text{cm}^{-3}$  (seeded in He) with beam velocity of  $\sim 2 \times 10^5 \text{ cm s}^{-1}$ , translational  
76 temperature of  $\sim 1 \text{ K}$  and rotational temperature of  $\sim 3 \text{ K}$ , thus cooling about  
77 half of the ortho- $CH_2O$  to the ground  $J = 0$  state.

78 2. *IR excitation (step 1).* Transition from the ground state  $|\nu = 0, J = 0, m_J = 0\rangle$  to  $|\nu', J, m_J = +J\rangle$  with  $\sigma_+$  light, and  $J = 1$  or 2 (Fig. 2).  $J = 1$

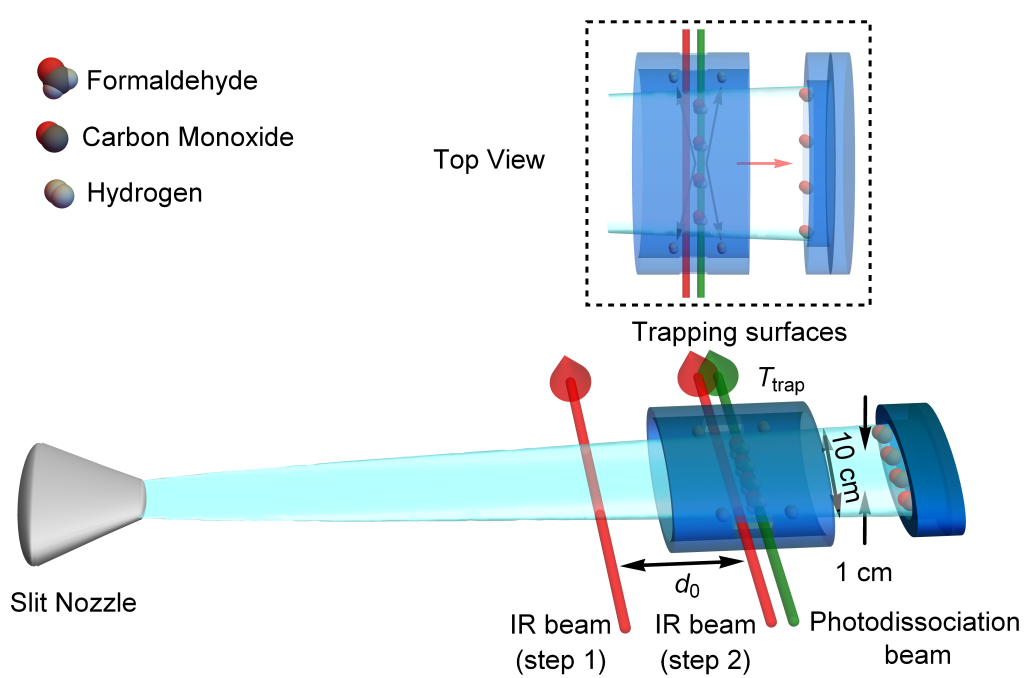


Figure 1: Experimental setup: supersonic expansion of  $\text{CH}_2\text{O}$  or  $\text{CH}_2\text{O}_2$  gas, followed by IR excitation (step 1), time evolution for time  $t_{\max} = d_0/v$ , then photodissociation, and trapping of polarized hydrogen or water photofragments at the cold surface.

is used for photoproducts with total nuclear spin  $I = 1$  (such as ortho H<sub>2</sub> or H<sub>2</sub>O), and  $J = 2$  for nuclei with total nuclear spin  $I = 3/2$  (such as HD or DT) or 2 (such as ortho D<sub>2</sub> or D<sub>2</sub>O), via successive two-photon absorption using STIRAP [25, 26, 27], for which population-transfer efficiency is typically > 90%. The absorption cross sections are  $\sim 10^{-16}$  cm<sup>2</sup> (for  $\nu' = \nu_2\nu_5$  at 4581.69 cm<sup>-1</sup>) and the column density of the ground state is  $3 \times 10^{16}$  cm<sup>-2</sup> so that greater than 99% of the 10<sup>21</sup> s<sup>-1</sup> IR photons are absorbed (as the 1 MHz laser linewidth is much narrower than the transition linewidth); for lower absorption cross sections, buildup cavities can be used to maximize IR absorption.

3. *Hyperfine polarization beating.* Subsequently, we leave the system to evolve freely, transferring rotational polarization to nuclear polarization, until the population of  $|\nu', J, m_J = -J\rangle$  (for  $I = 1$  or 2) or  $|\nu', J, m_J = -J + 1\rangle$  (for  $I = 3/2$ ) is maximized ( $t = t_{max}$ ). This state is 100% nuclear-spin polarized, due to the conservation of the total angular momentum projection along the quantization axis (hyperfine beatings under similar conditions have been demonstrated for HCl, HD, D<sub>2</sub> [18, 28, 29]). For CH<sub>2</sub>O, 16% of the population is 100% nuclear-spin-polarized and is transferred to the  $m_J = -1$  state (see Section 2). The total rotational energy transfer and depolarization cross section for the  $|J = 1, K = 0, M = 1\rangle$  state in CH<sub>2</sub>O is  $\sim 3 \times 10^{-15}$  cm<sup>2</sup> [30] (assuming a collision-energy-independent cross section). For collisional speeds of  $\sim 3 \times 10^3$  cm s<sup>-1</sup>, the de-excitation rate is  $\sim 10^{-11}$  cm<sup>3</sup> s<sup>-1</sup>, which, for 10<sup>15</sup> cm<sup>3</sup> densities, gives a de-excitation time of  $\sim 100$   $\mu$ s; therefore,  $t_{max}$  should be significantly less than 100  $\mu$ s.

4. *Hyperfine beating stopped.* At  $t = t_{max}$ , the beam enters a magnetic field of 1 mT, which stops the hyperfine beating [31].

5. *IR excitation (step 2) and photodissociation.* The transition  $|\nu', J, m_J = -J\rangle \rightarrow |\nu'', J = 0, m_J = 0\rangle$  (for  $I = 1$  or 2) or the  $|\nu', J, m_J = -1\rangle \rightarrow |\nu'', J = 1, m_J = +1\rangle$  (for  $I = 3/2$ ), with  $\sigma_+$  light, so that only the 100% nuclear-spin-polarized state is excited to the highest level. This fully-polarized state is then exclusively photodissociated by the photolysis laser (the lower states not having enough energy to photodissociate). For CH<sub>2</sub>O column density of  $3 \times 10^{16}$  cm<sup>-2</sup> and a photodissociation cross section of  $2.5 \times 10^{16}$  cm<sup>2</sup> (Fig. 4), more than 99% of the molecules are photodissociated, for laser fluxes of  $2 \times 10^{20}$  photons cm<sup>-2</sup> s<sup>-1</sup>. The photodissociation cross section for higher vibrational states is shifted to the green from the UV, due to the IR absorption energy of  $\sim 1$  eV. The photodissociation cross section of formic acid at 248 nm, for the CO + H<sub>2</sub>O channel, is about

118 1000 times smaller [32, 33], therefore a buildup cavity will be needed for  
119 the photodissociation laser, at 355 nm (for 2 IR photons) or 450 nm (for  
120 4 IR photons), to absorb a large percentage of the photolysis light. The  
121 produced H<sub>2</sub> molecules are in *J* states peaking at  $\sim 3$  [34], and hence a static  
122 magnetic field of  $\sim 1$  T is applied in the photodissociation region to prevent  
123 significant polarization exchange with *J* [35].

124 6. *Cold trapping.* More than 90% of the hydrogen or water isotopes  
125 reach trapping surfaces (that cover more than 90% of  $4\pi$  steradians), and  
126 are selectively trapped at these cold trapping surfaces with unity sticking  
127 probability [36] (the CO mainly follows the beam direction and is trapped  
128 elsewhere, with the unphotodissociated molecules (Fig. 1)).

129 The product of the efficiencies of the above steps 1-6 is  $\sim 10\%$ . Therefore,  
130  $10^{21}$  IR photons s<sup>-1</sup> will produce and trap an upper limit of  $10^{20}$  s<sup>-1</sup>  
131 spin-polarized molecules (this can be scaled up with larger laser powers  
132 and slit lengths). Future experiments will determine to what extent such  
133 production rates can be approached (e.g. the depolarization rates may be  
134 higher than assumed here, which will lower the production rate).

135 We describe in more detail why this method should surpass conventional  
136 methods by several orders of magnitude. Conventional molecular-beam  
137 separation methods are based on the differential deflection of the  
138 spin-projection states, from a beam with a cross sectional area *A*, velocity *v*,  
139 and density *ρ*, with large, localized B-field or E-field gradients, which limit  
140 *A* $\sim 1$  cm<sup>2</sup> to be small and localized. However, the beam density must be  
141 low enough so that the beam divergence, from collisions, is less than the  
142 differential deflections of the target spin-projection states. This constraint  
143 limits the beam density to  $\rho \sim 10^{11}$  cm<sup>-3</sup> for open-shell atoms [37]. The beam  
144 separation occurs over a distance of  $\sim 1$  m and on the ms timescale, with  
145 a beam velocity *v* typically in the range  $0.2\text{--}2.5 \times 10^5$  cm/s. The largest  
146 production rate (given by *Avρ*) for spin-polarized H atoms, which is the most  
147 favorable case, has been  $\sim 5 \times 10^{16}$  H/s [37]. For closed-shell molecules, the  
148 production rates are several orders of magnitude lower (as nuclear magnetic  
149 moments are  $\sim 10^3$  times smaller than electronic ones, due to the  $\sim 10^3$  larger  
150 mass).

151 In contrast, the polarization of nuclear spins in a molecular beam,  
152 via the IR-excitation method, occurs by the intramolecular transfer of  
153 rotational to nuclear polarization, via the hyperfine interaction on the  
154  $\mu$ s timescale, and thus does not require any type of beam separation or  
155 external inhomogeneous static fields. The lack of need to spatially separate

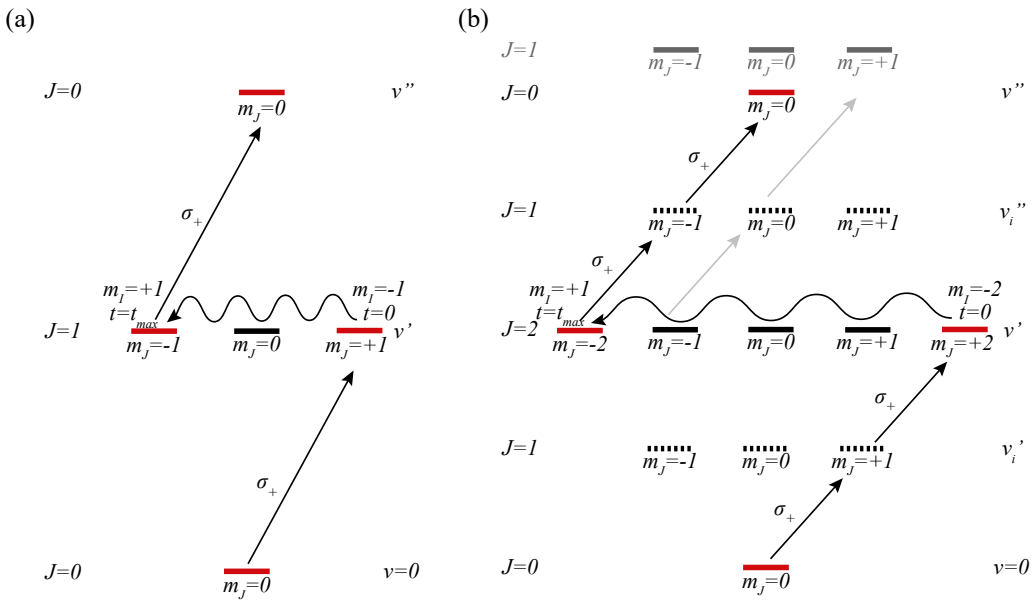


Figure 2: Excitation schemes for production of nuclear spin-polarized molecules with (a)  $I = 1$  (e.g. with constituent atoms of D or  $H_2$ ), and (b)  $I = 3/2$  or  $2$  (e.g. for HD, DT or  $D_2$ ). The squiggly arrows show rotational polarization reduction  $\Delta m_J = -2$  or  $-4$ , associated with nuclear spin increase  $\Delta m_I = +2$  or  $+4$  (for Figs. 2(a) or 2(b), respectively). Only 100% nuclear-spin-polarized molecules reach the upper state.

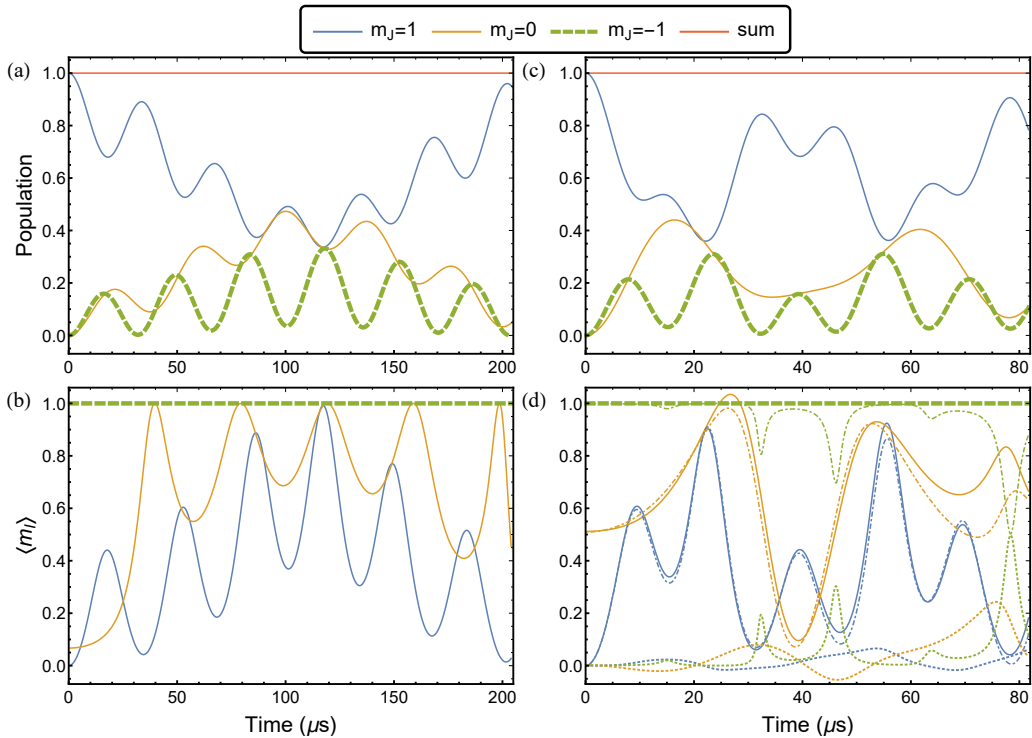


Figure 3: CH<sub>2</sub>O (a,b): Population and  $\langle m_I \rangle$  of  $m_J$  states as function of time. The  $m_J = -1$  state reaches 15.9% of the total population at  $\sim 16.2 \mu\text{s}$ . CHDO (c,d): Population and  $\langle m_I \rangle$  of  $m_J$  states as function of time. The solid lines (and the dashed thick line) correspond to the total nuclear spin projection, whereas the dash-dotted and dotted lines correspond to  $\langle m_{I_D} \rangle$ , and  $\langle m_{I_H} \rangle$  respectively. The  $m_J = -1$  state reaches 21.4% of the total population at  $7.9 \mu\text{s}$ . By that time, mainly the deuteron is polarized.

156 the spin-states in the molecular beam, the shorter polarization time, and  
 157 the ability to use a long slit expansion (not possible for conventional  
 158 beam-separation methods due to the inhomogeneous fields), allow the beam  
 159 area  $A$  and density  $\rho$  to be much higher than for beam-separation methods,  
 160 e.g.  $A \sim 10\text{-}100 \text{ cm}^2$ , and  $\rho \sim 10^{15} \text{ cm}^{-3}$ , which are 1-2 and 4 orders of  
 161 magnitude higher, respectively. This increase in  $A$  and  $\rho$  potentially allows  
 162 a total production rate  $Av\rho$  of up to  $\sim 10^{22} \text{ s}^{-1}$ . The production rate is  
 163 limited by the absorbed photons for the IR-excitation and photodissociation  
 164 steps: tabletop IR-excitation and photodissociation lasers producing  $\sim 10^{21}$   
 165 photons  $\text{s}^{-1}$  are available commercially; industrial-scale lasers can likely  
 166 reach higher. We note that related arguments were used to predict the  
 167 production of ultrahigh densities of spin-polarized hydrogen (SPH) atoms  
 168 from hydrogen halide photodissociation [38], and indeed  $10^{19}\text{-}10^{20}$  SPH were  
 169 observed [39, 40, 41], 8-9 orders higher than those from beam-separation  
 170 methods; therefore surpassing conventional beam-separation methods by  
 171 many orders of magnitude is not unprecedented.

## 172 **2. Production of spin-polarized $\text{H}_2$ (isotopes) from formaldehyde** 173 **IR excitation and photodissociation**

174 The IR-excitation method depends crucially on transferring a large  
 175 fraction of the population to the 100% nuclear-spin-polarized state, and in  
 176 short enough time ( $t_{max} \lesssim 30 \mu\text{s}$ ) to avoid significant depolarization under  
 177 these conditions. Below, we give a description of the calculation of the  
 178 polarization transfer and  $t_{max}$  for  $\text{CH}_2\text{O}$  and  $\text{CH}_2\text{O}_2$  isotopes.

The  $\text{CH}_2\text{O}$  ortho states ( $I = 1$ ) are described by  $K_{-1} = 1, 3, 5, \dots$  and the  
 para states by  $K_{-1} = 0, 2, 4, \dots$  in the notation  $J_{K_{-1}K_1}$  [42]. The hyperfine  
 hamiltonian matrix elements of the  $J = 1, K_{-1} = 1$  state can be written  
 as [43]:

$$\begin{aligned}
 E/h = & C(-1)^{I+J+F} [I(I+1)(2I+1)J(J+1)(2J+1)]^{1/2} \\
 & \times \left\{ \begin{array}{ccc} F & I & J \\ 1 & J & I \end{array} \right\} + D(-1)^{I+J+F} \left\{ \begin{array}{ccc} F & I & J \\ 2 & J & I \end{array} \right\} \\
 & \times \left[ \frac{(I+1)(2I+1)(2I+3)J(J+1)(2J+1)}{I(2I-1)(2J-1)(2J+3)} \right]^{1/2},
 \end{aligned} \tag{1}$$

where  $I = 1$  is the sum of proton spins,  $J$  the rotational angular momentum,  
 $F = J + I$  the total angular momentum,  $C$  the spin-rotation interaction

constant and  $D$  the spin-spin interaction constant. Substituting  $C(1_{11}) = -3.07$  kHz and  $D(1_{11}) = 8.87$  kHz [43] for the lower state  $K_1 = 1$  we obtain the hamiltonian matrix elements in the  $|F, m_F\rangle$  representation. After transforming to the  $|m_J, m_I\rangle$  basis as:

$$|m_J, m_I\rangle = \sum_{F, m_F} \langle F, m_F | m_J, m_I \rangle |F, m_F\rangle, \quad (2)$$

- 179 the hamiltonian is diagonalized to obtain the time evolved states [31] shown in  
 180 Fig. 3, where at  $t_{max} = 16.2$   $\mu$ s, 15.9% of the population has been transferred  
 181 to the  $m_J = -1$  state, which is always fully nuclear-spin-polarized (Fig. 3(b)).  
 182 The  $\langle m_I \rangle$  of each  $m_J$  state is plotted (Fig. 3(c,d)), giving the degree of nuclear  
 183 polarization for each state.

The same technique can be applied to singly deuterated formaldehyde, CHDO. The effective hyperfine hamiltonian for asymmetric top molecules with two (nonzero) nuclear spins is written as [46]:

$$\begin{aligned} H/h = & \frac{(eq_J Q)_D}{2I_D(2I_D - 1)J(2J - 1)} \left[ 3(\vec{I}_D \cdot \vec{J})^2 + \frac{3}{2}(\vec{I}_D \cdot \vec{J}) \right. \\ & - \vec{I}_D^2 \vec{J}^2 \left. \right] + \frac{d'_J}{J(2J - 1)} \left[ \frac{3}{2}(\vec{I}_D \cdot \vec{J})(\vec{I}_H \cdot \vec{J}) \right. \\ & + \frac{3}{2}(\vec{I}_H \cdot \vec{J})(\vec{I}_D \cdot \vec{J}) - (\vec{I}_H \cdot \vec{I}_D)\vec{J}^2 \left. \right] \\ & + C_H \vec{I}_H \cdot \vec{J} + C_D \vec{I}_D \cdot \vec{J}, \end{aligned} \quad (3)$$

- 184 where  $(eq_J Q)_D$ ,  $d'_J$ ,  $C_H$ , and  $C_D$  are the quadrupole interaction coupling  
 185 constant, the nuclear spin-spin interaction coupling constant, the proton and  
 186 deuteron spin-rotation interaction coupling constants, defined in [46].

- 187 The hyperfine structure of the  $1_{11}$  and  $1_{10}$  states of CHDO has been  
 188 studied by Tucker et al. [47]. We investigate the polarization dynamics of the  
 189  $1_{10}$ . Substituting  $C_H = -1.43$  kHz,  $C_D = 0.11$  kHz given in [47],  $d'_J = -0.54$   
 190 kHz which is calculated from molecular geometry (as it is presented in Fig.  
 191 2 of [48]), and  $(eq_J Q)_D = 17$  kHz, where the  $\chi_{aa}$ ,  $\chi_{bb}$ , and  $\chi_{cc}$  are taken from  
 192 Table V of [48]. Following the polarization scheme presented in Fig. 2(a), we  
 193 achieve 21.4% of population with 100% deuteron polarization at 7.9  $\mu$ s (see  
 194 Fig. 3(c,d)).

- 195 To produce nuclear-spin-polarized HD or DT molecules, a different  
 196 scheme (Fig. 2) is required. Starting with  $m_J=2$  ( $t=0$ ), at time  $t=t_{max}$   
 197 the population of the  $m_J = -1$  state is maximized (which has 100%

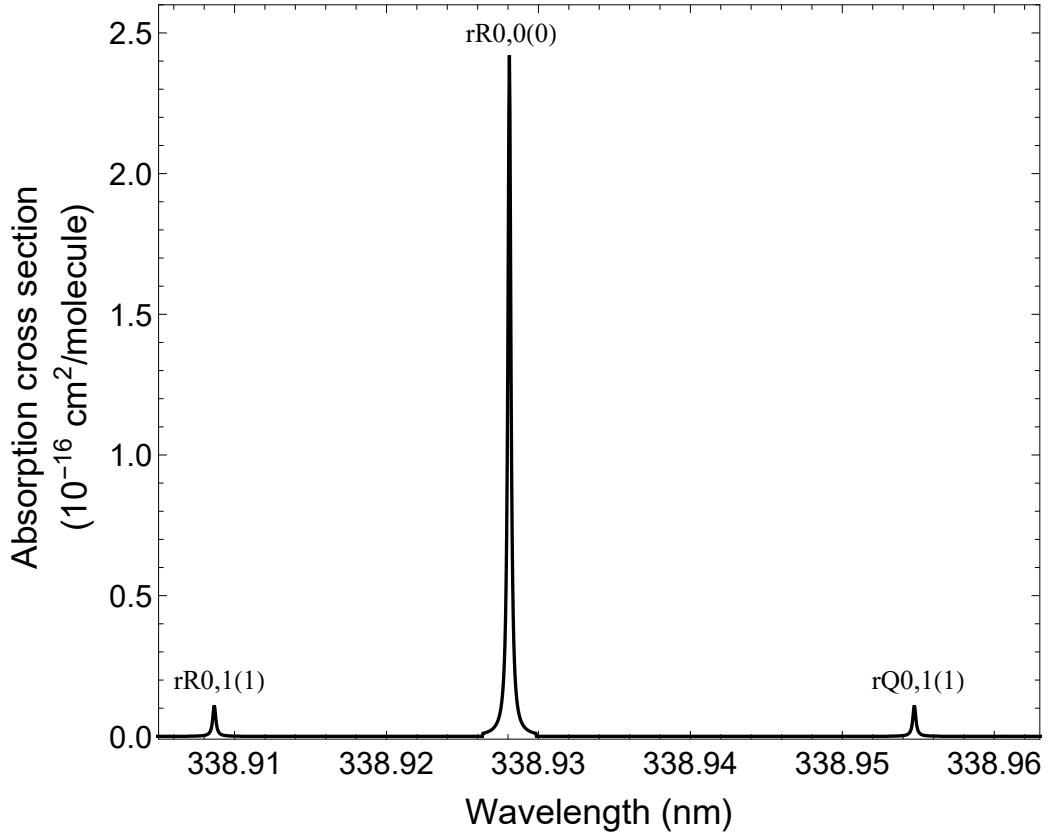


Figure 4: Simulated absorption spectrum of the  $2_0^1 4_0^1$  vibronic band of formaldehyde, using Gaussian and Lorentzian FWHM of  $0.003 \text{ cm}^{-1}$  and  $0.02 \text{ cm}^{-1}$ , respectively, and  $T = 1 \text{ K}$ . Relevant transitions are labeled. The absorption spectrum simulation of the  $2_0^1 4_0^1$  vibronic band was performed using the PGOPHER [44] program and the supporting material provided by [45].

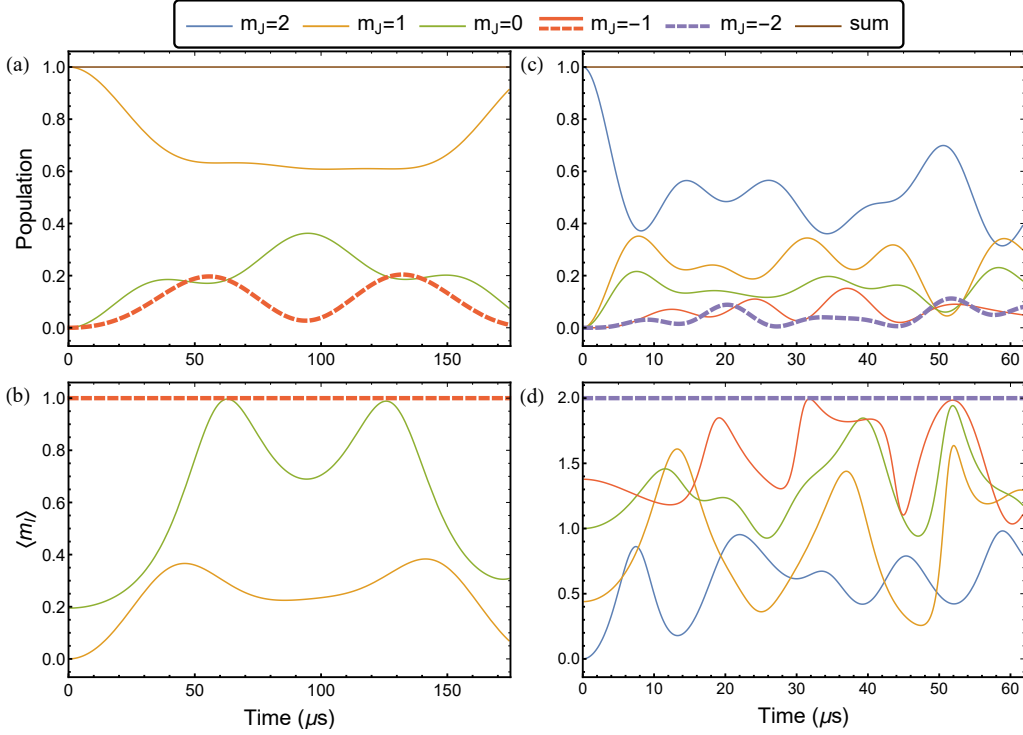


Figure 5:  $\text{CH}_2\text{O}_2$ (a,b): Population and total  $\langle m_I \rangle$  of  $m_J$  states as function of time. The  $m_J = -1$  state reaches 10% of the total population at  $33 \mu\text{s}$ .  $\text{CD}_2\text{O}_2$ (c,d): Population and total  $\langle m_I \rangle$  of  $m_J$  states as function of time. The  $m_J = -2$  state reaches 8.8% of the total population at  $\sim 20 \mu\text{s}$ .

nuclear-spin-polarization), and is then excited to the  $J=1$ ,  $m_J=+1$  state.  
 For the calculation of  $t_{max}$  the hyperfine constants for the  $J=2$  state are  
 needed. However, the  $C_{H,D}$  values found in the literature [46, 48, 47] are  
 not consistent and the  $M_{gg}^{H,D}$  have not been measured. Thus, we cannot  
 accurately determine  $t_{max}$  unless all the hyperfine constants of CHDO are  
 known. The proton spin-rotation constants are particularly required, because  
 they are mainly responsible for the polarization transfer to the proton. In the  
 case of D, the corresponding quadrupole coupling interaction is dominating.

206    **3. Production of spin-polarized H<sub>2</sub> (isotopes) from formic acid IR  
207    excitation and photodissociation**

Similar methods can be applied to ortho-trans-formic acid and isotopes. The effective hyperfine hamiltonian of formic acid (CH<sub>2</sub>O<sub>2</sub>) is written as [46, 49, 50]:

$$\begin{aligned} H/h = & C_{H_1} \vec{I}_1 \cdot \vec{J} + C_{H_2} \vec{I}_2 \cdot \vec{J} \\ & + \frac{d'_J}{J(2J-1)} \left[ \frac{3}{2} (\vec{I}_1 \cdot \vec{J})(\vec{I}_2 \cdot \vec{J}) \right. \\ & \left. + \frac{3}{2} (\vec{I}_2 \cdot \vec{J})(\vec{I}_1 \cdot \vec{J}) - (\vec{I}_1 \cdot \vec{I}_2) \vec{J}^2 \right], \end{aligned} \quad (4)$$

208 where  $I_1 = I_2 = 1/2$ ,  $d'_J = -\frac{6\mu_N^2 g_H^2}{(J+1)(2J+3)r^3} \sum_g \frac{r_g^2}{r^2} \langle J_g^2 \rangle - \frac{1}{3} J(J+1)$ ,  $C_{H_{1,2}} =$   
209  $\sum_g \frac{M_{gg}^{1,2} \langle J_g^2 \rangle}{J(J+1)}$ , and the constants labeled with 1 refer to the proton bounded to  
210 the carbon atom. For the 1<sub>11</sub> state,  $C_{H_1} = -3.8$  kHz,  $C_{H_2} = -4.1$  kHz [50],  
211 and  $d'_J = 1.8$  kHz [51, 52]. Figure 5 shows that the population of the  $m_J = -1$   
212 state reaches 10% at  $t \sim 33 \mu\text{s}$ , assuming 100% rotational polarization at  $t = 0$ .

The same technique, but for the  $|\nu', J = 2\rangle$  state (Fig. 2(b)) can be applied to double deuterated formic acid (CD<sub>2</sub>O<sub>2</sub>). The total wavefunction is symmetric in the exchange of nuclear spins  $I_1$  and  $I_2$ . In the case of  $K_{-1} = \text{even states}$ , the rotation wavefunction is symmetric, so the nuclear spin wavefunction must be symmetric, i.e.  $I = I_1 + I_2 = 0, 2$  (ortho states). Therefore, the non-zero hamiltonian matrix elements in the  $|J, I, F\rangle$  representation are [48]:

$$\begin{aligned} \langle J, I, F | H/h | J, I, F \rangle = & C_D \frac{A}{2J(J+1)} + \left[ a_Q \frac{3I(I+1) - 11}{(2I-1)(2I+3)} \right. \\ & \left. + a_S \frac{I(I+1) + 8}{2(2I-1)(2I+3)} \right] \frac{3A(A-1) - 4I(I+1)J(J+1)}{2J(J+1)(2J-1)(2J+3)}, \\ \langle J, I, F | H/h | J, I-2, F \rangle = & \frac{3(2a_Q - a_S)}{8J(J+1)(2J-1)(2J+3)(2I-1)} \\ & \times \sqrt{\frac{(I+3)(3-I)(I+2)(4-I)}{(2I-3)(2I+1)}} [(J-F+I)(J+F+I+1) \\ & \times (F+I-J)(J+F-I+1)(J-F+I-1)(J+F+I) \\ & \times (F+I-1-J)(J+F-I+2)]^{1/2}, \end{aligned} \quad (5)$$

213 where  $A = J(J + 1) + I(I + 1) - F(F + 1)$ . The constants  $a_Q$ ,  $a_S$ , and  $C_D$   
214 are the quadrupole interaction coupling constant, the nuclear spin-spin  
215 interaction coupling constant, and the spin-rotation interaction coupling  
216 constant, defined in [48].

217 Cazzoli et al. [53] measured the hyperfine constants  $\chi_{gg}$  and calculated  
218  $M_{gg}$  (see cc-pCVQZ calculation) using a semi-experimental equilibrium  
219 geometry. Figure 5(c,d) shows the hyperfine beats of the  $2_{21}$  state which  
220 is initially rotationally polarized. The values of the hyperfine constants are  
221  $a_Q = -152.85$  kHz,  $a_S = 0.24$  kHz, and  $C_D = -2.85$  kHz. The 8.8% of the  
222 population has been transferred to the  $m_J = -2$  state, at  $t_{max} = 20 \mu\text{s}$ . This  
223 state is always fully nuclear-spin-polarized (Fig. 5(c,d)).

224 This method of macroscopic production of polarized molecules can be  
225 generalized to several other systems, such as for spin-polarized O<sub>2</sub>, N<sub>2</sub>, NO,  
226 and <sup>13</sup>CO, from the IR-excitation and photodissociation of O<sub>3</sub>, N<sub>2</sub>O, NO<sub>2</sub>,  
227 and CO<sub>2</sub>.

228 This work is supported in part by the Hellenic Foundation for Research  
229 and Innovation (HFRI) and the General Secretariat for Research and  
230 Technology (GSRT), through the grant agreement No. HFRI-FM17-3709  
231 (project NUPOL).

## 232 References

- 233 [1] E. Steffens, W. Haeberli, Polarized gas targets, Rep. Prog. Phys. 66 (11)  
234 (2003) 1887–1935. doi:10.1088/0034-4885/66/11/r02.
- 235 [2] R. A. Green, R. W. Adams, S. B. Duckett, R. E. Mewis, D. C.  
236 Williamson, G. G. Green, The theory and practice of hyperpolarization  
237 in magnetic resonance using parahydrogen, Prog. Nucl. Mag. Res. Sp. 67  
238 (2012) 1 – 48. doi:<https://doi.org/10.1016/j.pnmrs.2012.03.001>.
- 239 [3] K. R. Keshari, D. M. Wilson, Chemistry and biochemistry of <sup>13</sup>C  
240 hyperpolarized magnetic resonance using dynamic nuclear polarization,  
241 Chem. Soc. Rev. 43 (2014) 1627–1659. doi:10.1039/C3CS60124B.
- 242 [4] M. H. Levitt, Singlet nuclear magnetic resonance, Annu.  
243 Rev. Phys. Chem. 63 (1) (2012) 89–105. doi:10.1146/  
244 annurev-physchem-032511-143724.

- 245 [5] E. ter Haar, W. G. Clark, Brute force nuclear polarization of D<sub>2</sub>, J. Low  
246 Temp. Phys. 94 (1994) 361–371. doi:10.1007/BF00754675.  
247 URL <https://doi.org/10.1007/BF00754675>
- 248 [6] G. Hupin, S. Quaglioni, P. Navrátil, Ab initio predictions for polarized  
249 deuterium-tritium thermonuclear fusion, Nat. Commun. 10 (2019) 351.
- 250 [7] M. Temporal, V. Brandon, B. Canaud, J. Didelez, R. Fedosejevs,  
251 R. Ramis, Ignition conditions for inertial confinement fusion targets with  
252 a nuclear spin-polarized DT fuel, Nucl. Fusion 52 (10) (2012) 103011.  
253 doi:10.1088/0029-5515/52/10/103011.  
254 URL <https://doi.org/10.1088%2F0029-5515%2F52%2F10%2F103011>
- 255 [8] K. Grigoryev, N. Chernov, R. Engels, I. Ivanov, S. Kiselev, E. Komarov,  
256 L. Kotchenda, P. Kravtsov, L. Kroell, A. Martyushov, M. Marusina,  
257 M. Mikirtychyants, N. Nikolaev, F. Rathmann, H. P. gen Schieck,  
258 S. Sherman, H. Ströher, V. Trofimov, A. Vasilyev, M. Vznuzdaev,  
259 Double polarized dd-fusion experiment, J. Phys. Conf. 295 (2011)  
260 012168. doi:10.1088/1742-6596/295/1/012168.  
261 URL <https://doi.org/10.1088/1742-6596/295/1/012168>
- 262 [9] R. M. Kulsrud, Application of Polarized Nuclei to Fusion, Springer US,  
263 Boston, MA, 1987, pp. 169–178. doi:10.1007/978-1-4757-5930-3\_14.  
264 URL [https://doi.org/10.1007/978-1-4757-5930-3\\_14](https://doi.org/10.1007/978-1-4757-5930-3_14)
- 266 [10] R. W. Moir, Hylife-II inertial fusion energy power plant design, Fusion  
267 Technol. 21 (3P2A) (1992) 1475–1486. doi:10.13182/FST92-A29929.  
268 URL <https://doi.org/10.13182/FST92-A29929>
- 269 [11] J. H. Ardenkjaer-Larsen, B. Fridlund, A. Gram, G. Hansson,  
270 L. Hansson, M. H. Lerche, R. Servin, M. Thaning, K. Golman, Increase  
271 in signal-to-noise ratio of > 10,000 times in liquid-state NMR., Proc.  
272 Natl. Acad. Sci. USA 100 (18) (2003) 10158–10163. doi:10.1073/pnas.  
273 1733835100.  
274 URL <https://doi.org/10.1073/pnas.1733835100>
- 275 [12] A. C. Pinon, A. Capozzi, J. H. Ardenkjær-Larsen, Hyperpolarized  
276 water through dissolution dynamic nuclear polarization with  
277 UV-generated radicals., Commun. Chem. 3 (2020) 57. doi:

- 278        10.1038/s42004-020-0301-6.  
279        URL <https://doi.org/10.1038/s42004-020-0301-6>
- 280 [13] Y. Shestakov, D. Nikolenko, I. Racheck, D. Toporkov, A. Yurchenko,  
281        Nuclear-polarized hydrogen/deuterium molecular source, Phys. Part.  
282        Nuclei 50 (5) (2019) 513–519. doi:10.1134/S1063779619050204.
- 283 [14] T. Kravchuk, M. Reznikov, P. Tichonov, N. Avidor, Y. Meir,  
284        A. Bekkerman, G. Alexandrowicz, A magnetically focused molecular  
285        beam of ortho-water, Science 331 (6015) (2011) 319–321. doi:10.1126/  
286        science.1200433.  
287        URL <https://science.sciencemag.org/content/331/6015/319>
- 288 [15] D. A. Horke, Y.-P. Chang, K. Długołęcki, J. Küpper, Separating para  
289        and ortho water, Angew. Chem. Int. Ed. 53 (44) (2014) 11965–11968.  
290        doi:10.1002/anie.201405986.  
291        URL <https://onlinelibrary.wiley.com/doi/abs/10.1002/anie.201405986>
- 293 [16] T. P. Rakitzis, Highly spin-polarized atoms and molecules from  
294        rotationally state-selected molecules, Phys. Rev. Lett. 94 (2005) 083005.  
295        doi:10.1103/PhysRevLett.94.083005.  
296        URL <https://link.aps.org/doi/10.1103/PhysRevLett.94.083005>
- 297 [17] L. Rubio-Lago, D. Sofikitis, A. Koubenakis, T. P. Rakitzis,  
298        Time-dependent polarization transfer from molecular rotation to nuclear  
299        spin, Phys. Rev. A 74 (2006) 042503. doi:10.1103/PhysRevA.74.042503.  
300  
301        URL <https://link.aps.org/doi/10.1103/PhysRevA.74.042503>
- 302 [18] D. Sofikitis, L. Rubio-Lago, M. R. Martin, Davida J. Ankeny Brown,  
303        Nathaniel C.-M. Bartlett, R. N. Zare, T. P. Rakitzis, Preparation of  
304        highly polarized nuclei: Observation and control of time-dependent  
305        polarization transfer from H<sup>35</sup>Cl molecular rotation to <sup>35</sup>Cl nuclear spin,  
306        Phys. Rev. A 76 (2007) 012503. doi:10.1103/PhysRevA.76.012503.  
307        URL <https://link.aps.org/doi/10.1103/PhysRevA.76.012503>
- 308 [19] D. Sofikitis, L. Rubio-Lago, M. R. Martin, D. J. Ankeny Brown, N. C.-M.  
309        Bartlett, A. J. Alexander, R. N. Zare, T. P. Rakitzis, Optical control  
310        of ground-state atomic orbital alignment: Cl (<sup>2</sup>P<sub>3/2</sub>) atoms from HCl

- 311 (v=2,J=1) photodissociation, J. Chem. Phys. 127 (14) (2007) 144307.  
312 doi:10.1063/1.2772272.  
313 URL <https://doi.org/10.1063/1.2772272>
- 314 [20] R. Engels, M. Gaißer, R. Gorski, K. Grigoryev, M. Mikirtychyants,  
315 A. Nass, F. Rathmann, H. Seyfarth, H. Ströher, P. Weiss, L. Kochenda,  
316 P. Kravtsov, V. Trofimov, N. Tschernev, A. Vasilyev, M. Vznuzdaev,  
317 H. P. g. Schieck, Production of hyperpolarized H<sub>2</sub> molecules from  
318 → h atoms in gas-storage cells, Phys. Rev. Lett. 115 (2015) 113007.  
319 doi:10.1103/PhysRevLett.115.113007.  
320 URL <https://link.aps.org/doi/10.1103/PhysRevLett.115.113007>
- 321
- 322 [21] S. B. Mirov, I. S. Moskalev, S. Vasilyev, V. Smolski, V. V.  
323 Fedorov, D. Martyshkin, J. Peppers, M. Mirov, A. Dergachev,  
324 V. Gapontsev, Frontiers of mid-IR lasers based on transition metal  
325 doped chalcogenides, IEEE J. Sel. Top. Quantum Electron. 24 (5) (2018)  
326 1–29. doi:10.1109/JSTQE.2018.2808284.
- 327 [22] A. G. Suits, S. D. Chambreau, S. A. Lahankar, State-correlated DC  
328 slice imaging of formaldehyde photodissociation: roaming atoms and  
329 multichannel branching, Int. Rev. Phys. Chem. 26 (4) (2007) 585–607.  
330 doi:10.1080/01442350701589908.  
331 URL <https://doi.org/10.1080/01442350701589908>
- 332 [23] Y. Ma, J. Liu, F. Li, F. Wang, T. N. Kitsopoulos, Roaming dynamics  
333 in the photodissociation of formic acid at 230 nm, J. Phys. Chem. A  
334 123 (17) (2019) 3672–3677. doi:10.1021/acs.jpca.9b00724.  
335 URL <https://doi.org/10.1021/acs.jpca.9b00724>
- 336 [24] D. J. Nesbitt, High-resolution, direct infrared laser absorption  
337 spectroscopy in slit supersonic jets: Intermolecular forces and  
338 unimolecular vibrational dynamics in clusters, Annual Review of  
339 Physical Chemistry 45 (1) (1994) 367–399. arXiv:<https://doi.org/10.1146/annurev.pc.45.100194.002055>, doi:10.1146/annurev.pc.45.100194.002055.  
340  
341 URL <https://doi.org/10.1146/annurev.pc.45.100194.002055>
- 342
- 343 [25] K. Bergmann, H.-C. Nägerl, C. Panda, G. Gabrielse, E. Miloglyadov,  
344 M. Quack, G. Seyfang, G. Wichmann, S. Ospelkaus, A. Kuhn, S. Longhi,

- 345 A. Szameit, P. Pirro, B. Hillebrands, X.-F. Zhu, J. Zhu, M. Drewsen,  
346 W. K. Hensinger, S. Weidt, T. Halfmann, H.-L. Wang, G. S. Paraoanu,  
347 N. V. Vitanov, J. Mompart, T. Busch, T. J. Barnum, D. D. Grimes,  
348 R. W. Field, M. G. Raizen, E. Narevicius, M. Auzinsh, D. Budker,  
349 A. Pálffy, C. H. Keitel, Roadmap on STIRAP applications, *J. Phys. B: At. Mol. Opt. Phys.* 52 (20) (2019) 202001. doi:10.1088/1361-6455/ab3995.  
350  
351 URL <https://doi.org/10.1088/1361-6455/ab3995>
- 352 [26] N. V. Vitanov, A. A. Rangelov, B. W. Shore, K. Bergmann, Stimulated raman adiabatic passage in physics, chemistry, and beyond, *Rev. Mod. Phys.* 89 (2017) 015006. doi:10.1103/RevModPhys.89.015006.  
353  
354 URL <https://link.aps.org/doi/10.1103/RevModPhys.89.015006>
- 355 [27] K. Bergmann, N. V. Vitanov, B. W. Shore, Perspective: Stimulated raman adiabatic passage: The status after 25 years, *J. Chem. Phys.* 142 (17) (2015) 170901. doi:10.1063/1.4916903.  
356  
357 URL <https://doi.org/10.1063/1.4916903>
- 358 [28] N. C.-M. Bartlett, D. J. Miller, R. N. Zare, A. J. Alexander, D. Sofikitis,  
359 T. P. Rakitzis, Time-dependent depolarization of aligned HD molecules,  
360 *Phys. Chem. Chem. Phys.* 11 (2009) 142–147. doi:10.1039/B814133A.  
361  
362 URL <http://dx.doi.org/10.1039/B814133A>
- 363 [29] N. C.-M. Bartlett, J. Jankunas, R. N. Zare, J. A. Harrison,  
364 Time-dependent depolarization of aligned D<sub>2</sub> caused by hyperfine coupling, *Phys. Chem. Chem. Phys.* 12 (2010) 15689–15694. doi:  
365 10.1039/C0CP00518E.  
366  
367 URL <http://dx.doi.org/10.1039/C0CP00518E>
- 368 [30] L. F. Phillips, Theoretical cross-sections for resonant exchange of  
369 rotational energy in a stark field, *Chem. Phys. Lett.* 291 (1) (1998)  
370 94–100. doi:[https://doi.org/10.1016/S0009-2614\(98\)00524-7](https://doi.org/10.1016/S0009-2614(98)00524-7).  
371  
372 URL <https://www.sciencedirect.com/science/article/pii/S0009261498005247>
- 373 [31] C. S. Kannis, G. E. Katsoprinakis, D. Sofikitis, T. P. Rakitzis,  
374 Nuclear-spin-polarization dynamics of H<sub>2</sub>, D<sub>2</sub>, and HD molecules in  
375 magnetic fields, *Phys. Rev. A* 98 (2018) 043426. doi:10.1103/  
376  
377

- 378                   PhysRevA.98.043426.  
379                   URL <https://link.aps.org/doi/10.1103/PhysRevA.98.043426>
- 380 [32] D. Singleton, G. Paraskevopoulos, R. Irwin, UV absorption  
381 cross-sections of the monomer and dimer of formic acid, J.  
382 Photochem. 37 (2) (1987) 209 – 216. doi:[https://doi.org/10.1016/0047-2670\(87\)85001-3](https://doi.org/10.1016/0047-2670(87)85001-3).  
383                   URL <http://www.sciencedirect.com/science/article/pii/0047267087850013>
- 386 [33] S. Maeda, T. Taketsugu, K. Ohno, K. Morokuma, From roaming  
387 atoms to hopping surfaces: Mapping out global reaction routes in  
388 photochemistry, J. Am. Chem. Soc. 137 (10) (2015) 3433–3445. doi:  
389 [10.1021/ja512394y](https://doi.org/10.1021/ja512394y).  
390                   URL <https://doi.org/10.1021/ja512394y>
- 391 [34] T. J. Butenhoff, K. L. Carleton, C. B. Moore, Photodissociation  
392 dynamics of formaldehyde: H<sub>2</sub> rotational distributions and product  
393 quantum state correlations, J. Chem. Phys. 92 (1) (1990) 377–393.  
394 doi:[10.1063/1.458440](https://doi.org/10.1063/1.458440).  
395                   URL <https://doi.org/10.1063/1.458440>
- 396 [35] R. Engels, H. Awwad, K. Grigoryev, L. Huxold, M. Martic, A. Rolofs,  
397 W. Sartison, H. Ströher, M. Büscher, A. Vasilyev, L. Kochenda,  
398 P. Kravtsov, V. Trofimov, M. Vznudaev, Production and storage of  
399 polarized H<sub>2</sub>, D<sub>2</sub>, and HD molecules, PoS PSTP2017 (2018) 033. doi:  
400 [10.22323/1.324.0033](https://doi.org/10.22323/1.324.0033).
- 401 [36] T. R. Govers, L. Mattera, G. Scoles, Molecular beam experiments  
402 on the sticking and accommodation of molecular hydrogen on a  
403 low-temperature substrate, J. Chem. Phys. 72 (10) (1980) 5446–5455.  
404 doi:[10.1063/1.439013](https://doi.org/10.1063/1.439013).  
405                   URL <https://doi.org/10.1063/1.439013>
- 406 [37] A. Nass, C. Baumgarten, B. Braun, G. Ciullo, G. Court, P. Dalpiaz,  
407 A. Golendukhin, G. Graw, W. Haeberli, M. Henoch, R. Hertenberger,  
408 N. Koch, H. Kolster, P. Lenisa, H. Marukyan, M. Raithel, D. Reggiani,  
409 K. Rith, M. Simani, E. Steffens, J. Stewart, P. Tait, T. Wise, The  
410 HERMES polarized atomic beam source, Nucl. Instrum. Meth. A 505 (3)

- 411 (2003) 633 – 644. doi:[https://doi.org/10.1016/S0168-9002\(03\)  
412 00986-0.](https://doi.org/10.1016/S0168-9002(03)00986-0)
- 413 [38] D. Sofikitis, P. Glodic, G. Koumarianou, H. Jiang, L. Bougas, P. C.  
414 Samartzis, A. Andreev, T. P. Rakitzis, Highly nuclear-spin-polarized  
415 deuterium atoms from the UV photodissociation of deuterium iodide,  
416 Phys. Rev. Lett. 118 (2017) 233401. doi:[10.1103/PhysRevLett.118.  
417 233401.](https://doi.org/10.1103/PhysRevLett.118.233401)  
418 URL [https://link.aps.org/doi/10.1103/PhysRevLett.118.  
419 233401](https://link.aps.org/doi/10.1103/PhysRevLett.118.233401)
- 420 [39] D. Sofikitis, C. S. Kannis, G. K. Boulogiannis, T. P. Rakitzis,  
421 Ultrahigh-density spin-polarized H and D observed via magnetization  
422 quantum beats, Phys. Rev. Lett. 121 (2018) 083001. doi:  
423 [10.1103/PhysRevLett.121.083001.](https://doi.org/10.1103/PhysRevLett.121.083001)  
424 URL [https://link.aps.org/doi/10.1103/PhysRevLett.121.  
425 083001](https://link.aps.org/doi/10.1103/PhysRevLett.121.083001)
- 426 [40] A. K. Spiliotis, M. Xygkis, M. E. Koutrakis, K. Tazes, G. K.  
427 Boulogiannis, C. S. Kannis, G. E. Katsoprinakis, D. Sofikitis, T. P.  
428 Rakitzis, Ultrahigh-density spin-polarized hydrogen isotopes from the  
429 photodissociation of hydrogen halides: new applications for laser-ion  
430 acceleration, magnetometry, and polarized nuclear fusion, Light Sci.  
431 Appl. 10 (2021) 35. doi:[10.1038/s41377-021-00476-y.](https://doi.org/10.1038/s41377-021-00476-y)  
432 URL <https://doi.org/10.1038/s41377-021-00476-y>
- 433 [41] A. K. Spiliotis, M. Xygkis, M. Koutrakis, D. Sofikitis, T. P. Rakitzis,  
434 Depolarization of spin-polarized hydrogen via spin-exchange collisions  
435 with chlorine atoms at ultrahigh densityarXiv:[2101.02675](https://arxiv.org/abs/2101.02675).
- 436 [42] P. C. Cross, R. M. Hainer, G. W. King, The asymmetric rotor II.  
437 calculation of dipole intensities and line classification, J. Chem. Phys.  
438 12 (6) (1944) 210–243. doi:[10.1063/1.1723935.](https://doi.org/10.1063/1.1723935)  
439 URL <https://doi.org/10.1063/1.1723935>
- 440 [43] S. Kukolich, D. Ruben, Measurement of H<sub>2</sub>CO hyperfine structure  
441 with a two-cavity maser, J. Mol. Spectrosc. 38 (1) (1971) 130 – 135.  
442 doi:[https://doi.org/10.1016/0022-2852\(71\)90098-1.](https://doi.org/10.1016/0022-2852(71)90098-1)  
443 URL [http://www.sciencedirect.com/science/article/pii/  
444 0022285271900981](http://www.sciencedirect.com/science/article/pii/0022285271900981)

- 445 [44] C. M. Western, PGOPHER, a program for rotational,  
446 vibrational and electronic spectra, University of Bristol, 2005,  
447 <http://pgopher.chm.bris.ac.uk>.
- 448 [45] C. A. Smith, F. D. Pope, B. Cronin, C. B. Parkes, A. J. Orr-Ewing,  
449 Absorption cross sections of formaldehyde at wavelengths from 300  
450 to 340 nm at 294 and 245 K, *J. Phys. Chem. A* 110 (41) (2006)  
451 11645–11653. doi:[10.1021/jp063713y](https://doi.org/10.1021/jp063713y).  
452 URL <https://doi.org/10.1021/jp063713y>
- 453 [46] P. Thaddeus, L. C. Krisher, J. H. N. Loubser, Hyperfine structure in the  
454 microwave spectrum of HDO, HDS, CH<sub>2</sub>O, and CHDO: Beams-maser  
455 spectroscopy on asymmetric-top molecules, *J. Chem. Phys.* 40 (2) (1964)  
456 257–273. doi:[10.1063/1.1725107](https://doi.org/10.1063/1.1725107).  
457 URL <https://doi.org/10.1063/1.1725107>
- 458 [47] K. Tucker, G. Tomasevich, Deuteron quadrupole coupling in  
459 formaldehyde, *J. Mol. Spectrosc.* 48 (3) (1973) 475 – 478.  
460 doi:[https://doi.org/10.1016/0022-2852\(73\)90111-2](https://doi.org/10.1016/0022-2852(73)90111-2).  
461 URL <http://www.sciencedirect.com/science/article/pii/0022285273901112>
- 463 [48] W. H. Flygare, Experimental determination of the field gradient at the  
464 deuteron in formaldehyde, *J. Chem. Phys.* 41 (1) (1964) 206–214. doi:  
465 10.1063/1.1725624.  
466 URL <https://doi.org/10.1063/1.1725624>
- 467 [49] J. Chardon, C. Genty, D. Guichon, J. Theobald, rf spectrum and  
468 hyperfine structure of formic acid, *J. Chem. Phys.* 64 (4) (1976)  
469 1437–1441. doi:[10.1063/1.432412](https://doi.org/10.1063/1.432412).  
470 URL <https://doi.org/10.1063/1.432412>
- 471 [50] Cazzoli, G., Puzzarini, C., Stopkowicz, S., Gauss, J., Hyperfine structure  
472 in the rotational spectra of trans-formic acid: Lamb-dip measurements  
473 and quantum-chemical calculations\*, *A&A* 520 (2010) A64. doi:[10.1051/0004-6361/201014787](https://doi.org/10.1051/0004-6361/201014787).  
474 URL <https://doi.org/10.1051/0004-6361/201014787>
- 476 [51] J. Bellet, A. Deldalle, C. Samson, G. Stenbeckeliers, R. Wertheimer,  
477 Étude du spectre de rotation de la molécule d'acide formique: B. Étude

- 478 de quelques substituons isotopiques. application à la détermination  
479 de la structure de la molécule, J. Mol. Struct. 9 (1) (1971) 65 – 75.  
480 doi:[https://doi.org/10.1016/0022-2860\(71\)85007-X](https://doi.org/10.1016/0022-2860(71)85007-X).  
481 URL <http://www.sciencedirect.com/science/article/pii/002228607185007X>
- 483 [52] W. H. Hocking, The other rotamer of formic acid, cis-HCOOH1,  
484 Z. Naturforsch. A 31 (9) (1976) 1113 – 1121. doi:<https://doi.org/10.1515/zna-1976-0919>.  
485 URL <https://www.degruyter.com/view/journals/zna/31/9/article-p1113.xml>
- 488 [53] G. Cazzoli, C. Puzzarini, S. Stopkowicz, J. Gauss, The rotational  
489 spectrum of trans-DCOOD: Lamb-dip measurements, THz spectroscopy  
490 and quantum-chemical calculations, Chem. Phys. Lett. 502 (1) (2011)  
491 42 – 47. doi:<https://doi.org/10.1016/j.cplett.2010.12.023>.  
492 URL <http://www.sciencedirect.com/science/article/pii/S0009261410016076>  
493